Multitree Search for Multisatellite Responsiveness Scheduling Considering Orbital Maneuvering

ZHONG ZHANG
NAN ZHANG
YIFEI JIAO
HEXI BAOYIN
JUNFENG LI
Tsinghua University, Beijing, China

Rapid and responsive Earth observation satellites enable the evaluation of disaster risk, improve relief effectiveness, and reduce suffering and fatalities in the event of sudden disaster events. One promising method for responsive space satellites is orbital maneuvering. This article describes a multitree search framework for multisatellite responsiveness scheduling considering orbital maneuvering, where multiple ground targets are cooperatively observed by multiple observation satellites over a short period of time. Based on the traditional tree search, the proposed method constructs multiple trees and distributes all the targets to multiple satellites, allowing the observation sequence of a single satellite to be optimized. To apply the tree search algorithm, a tree node collection (TNC) composed of the corresponding nodes in multiple trees is used to represent the state of each satellite. Before the expansion phase, one specific node in the TNC is determined for later expansion. A beam search is then used to optimize the observation sequence. Ground-track adjustment techniques using impulse maneuver are considered for visiting a given target. The proposed framework is more effective than other algorithms and achieves a better performance than the previous best method in a typical multisatellite responsiveness scheduling scenario.

Manuscript received May 24, 2021; revised September 10, 2021 and November 13, 2021; released for publication November 17, 2021. Date of publication November 22, 2021; date of current version June 9, 2022.

DOI. No. 10.1109/TAES.2021.3129723

Refereeing of this contribution was handled by B. Jones.

This work was supported in part by the National Natural Science Foundation of China under Grant 11872223.

Authors' addresses: The authors are with the School of Aerospace Engineering, Tsinghua University, Beijing 100084 China, E-mail: (zhongzh19@mails.tsinghua.edu.cn; n-zhang19@mails.tsinghua.edu.cn; jiaoyf20@mails.tsinghua.edu.cn, baoyin@tsinghua.edu.cn; lijunf@tsinghua.edu.cn). *(Corresponding author: Junfeng Li.)*

I. INTRODUCTION

Earth observation satellites (EOSs) provide a global perspective and reduce the informational uncertainties after disasters that may hinder the emergency response, such as limited, incomplete, and often contradictory ground information. From 2000 to 2020, more than 1800 such incidents occurred (e.g., the Indian Ocean tsunami in 2004 and the Wenchuan earthquake in 2008), and satellite monitoring was increasingly utilized for global assessments of the disaster situation [1]. Thus, multisatellite emergency response is a global trend. In such emergencies, reasonable organization of the available satellite operations is of paramount importance in accomplishing rescue and aid missions.

The orbits and sensors of EOSs usually control the ground resolution (orbit altitude), area coverage, and revisit time. Essentially, the resolution and revisit time are conflicting factors for which engineers have attempted to find a reasonable tradeoff [2]. However, in multisatellite emergency response missions, rapid response and high resolution are both key factors. The traditional satellite imaging scheduling problem mainly focuses on the attitude maneuver planning in the daily observation mission of EOSs [3], [4], and many algorithms for better schedules have been proposed in an attempt to satisfy observation requests. Lemaître *et al.* [5] considered a simplified version of the agile satellites scheduling problem and used four existing algorithms to solve it: a greedy algorithm, a dynamic programming algorithm, a constraint programming approach, and a local search method. Wang *et al.* [6] established a task merging graph model and proposed a dynamic task-merging scheduling algorithm for emergency tasks. Other algorithms, such as the genetic algorithm (GA) [7], [8], differential evolution (DE) [9], ant colony optimization (ACO) algorithm [10], [11], and tabu search [12], have been extensively studied to satisfy the various constraints and address the satellite imaging scheduling problem effectively and efficiently. Nevertheless, the aforementioned algorithms all focus on the attitude maneuvering of EOSs, and there is an urgent need for more observation information and high quality pictures in multisatellite emergency response missions. Satellites cannot achieve faster response speeds by relying on attitude maneuvering alone. Engineers and the emergency response community have, therefore, considered the potential to accelerate the response speed using orbital maneuvering [13].

Research on EOS ground tracks can be classified into two main categories: the design of orbit ground tracks and ground-track adjustments. For the design of orbit ground tracks, Pontani *et al.* [14] introduced a method for designing low Earth orbit (LEO) satellite constellations in circular, repeating orbits for local observations. Abdelkhalik *et al.* [15] used a GA to find the natural orbit that observes all required sites without maneuvering. Mortari *et al.* [16], [17] established the original theory of flower constellations and its derivative necklace theory to minimize the number of satellites required for real-time coverage. However, these orbital mechanics studies are applied in the mission design

phase, and once the satellites have been launched it is too late to specify a new target. In this article, the main focus is on using existing satellite platforms to achieve the required observations.

In terms of ground-track adjustments, Zhu *et al.* [18] used a hybrid particle swarm optimization (PSO) and DE algorithm to address the problem of multiple satellites, where there is a single target and all satellites have the same final orbit. Co *et al.* [19] quantified that existing technology with standard propellant budgets, both chemical and electrical propulsion systems, could enable suitable maneuvering to respond to user's needs in a timely fashion. Furthermore, an algorithm has been developed to compute the requirements for an overflight of any terrestrial target (within the coverage area) using a single LEO satellite with electric propulsion [20]. Zhang *et al.* [21] established an approximate model that helps researchers understand the effects of impulsive maneuvers on an arbitrary point of the ground track. Zhang *et al.* [22] later introduced approximate analytical solutions for single and dual coplanar impulsive maneuvers enabling any given target to be observed by overflight or a conical sensor. Guelman *et al.* [23] introduced a simple closed-loop orbit control solution using low-thrust electric propulsion that does not require precomputed orbit commands, and Mok *et al.* [24] proposed a near-optimal impulsive control method for overflying ground targets. Zhang *et al.* [25] recently analyzed the reachable domain of the ground track under a single upper bounded impulse.

The aforementioned studies on ground-track adjustments are mainly devoted to finding maneuvering solutions for observing one target. There are very few studies on the maneuver strategy for observing multiple targets. Lin *et al.* [26] studied the ground-track adjustment problems for overflying one, two, and three ground targets with a single coplanar impulse. Mok *et al.* [24] considered the observation of three targets using explicit enumeration, while two studies have considered ten random targets with a deterministic order of observation [20], [23]. When the number of targets increases, scheduling algorithms are needed to effectively reduce the fuel consumption and revisit time. (As a practical instance, after the MH370 air accident, China deployed ten satellites to survey the South China Sea in an attempt to locate the aircraft. Such a problem is technically challenging because of the strict time constraints and vast search space, whereupon the curse of dimensionality appears.)

This article presents a multitree search (MTS) framework for the multisatellite responsiveness scheduling problem considering orbital maneuvering. The traditional tree search framework is extended by constructing multiple trees, and a tree node collection (TNC) is used to represent the state of each satellite. Therefore, distributing all of the targets to multiple satellites and optimizing the observation sequence of each satellite can be executed simultaneously. In addition, existing ground-track adjustment techniques to overfly the next target using impulse maneuver are considered as the number of nodes expands. This framework is used to derive a new solution to task 1 of the 11th China trajectory optimization competition (CTOC11) that is better than the winning solution, demonstrating the effectiveness of the proposed approach.

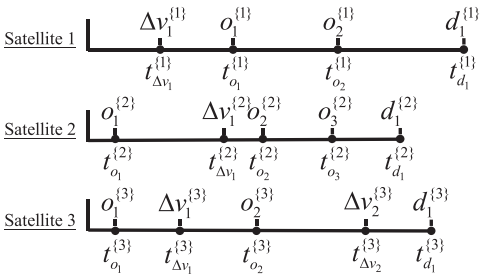

Fig. 1. Illustration of multisatellite responsiveness scheduling mission.

The rest of this article is organized as follows. In Section II, the optimization problem and dynamics model are introduced. In Section III, the tree-based search framework is described in detail. Sections IV and V demonstrate the effectiveness of the proposed framework through a comparison with other algorithms and a simulation of task 1 from CTOC11. Finally, Section VI concludes this article.

II. PROBLEM DESCRIPTION

In multisatellite responsiveness scheduling missions, the objective is to utilize multiple satellites to observe all the specific ground targets as quickly as possible. In this article, it is assumed that the satellites are equipped with high-thrust chemical thrusters to apply orbit maneuvers, and the maneuvering process is considered as an instantaneous impulse. Considering the capability of satellites, the propellant for maneuvers is limited, while the number of targets is large. Limited by the storage capability of the satellites, the observation data need to be transmitted during the mission. With such crucial conditions, it is vital to exploit the ability for cooperative observation by the satellites.

An example of such a scheduling mission is shown in Fig. 1, where three satellites are scheduled to observe seven targets. The superscript k denotes the kth satellite, where $k = 1, 2$, and 3 in this example, $d_i^{\{k\}}$ is the ith data transmission by the kth satellite, $\Delta v_i^{\{k\}}$ is the ith impulse of the kth satellite, $o_j^{\{k\}}$ is the jth observation made by the kth satellite, and t is the corresponding epoch of the aforementioned actions; the superscripts and subscripts of t are used in the same way. Reflecting on a general case in which K satellites are used to observe N targets $\{o_1, o_2, \ldots, o_N\}$, further information about the problem is described in the following subsections.

Reflecting on a general case in which K satellites are used to observe N targets $\{o_1, o_2, \ldots, o_N\}$, further information about the problem is described in the following subsections.

A. Environment and Dynamics

Gravity, the Earth's oblateness perturbation (J_2 effect), and atmospheric drag are considered in the orbital dynamics of observation satellites. This dynamic model is the same as the CTOC11 problem, so it is convincing to validate

the proposed methods by comparing the simulation results given in Section V. In the Earth-centered inertial (ECI) frame, the dynamic equation of the observation satellites is

$$\ddot{\boldsymbol{r}} = -\frac{\mu}{r^3}\boldsymbol{r} + \boldsymbol{a}_{J_2} + \boldsymbol{a}_{\mathrm{d}} \tag{1}$$

where $\boldsymbol{r} = [x, y, z]^{\mathrm{T}}$ is the position vector of the observation satellites in the ECI frame, $r = \|\boldsymbol{r}\|$, $\mu = 398600.4415\,\mathrm{km}^3/\mathrm{s}^2$ is the gravitational parameter of the Earth, $\boldsymbol{a}_{J_2}$ is the J_2 perturbation acceleration, and $\boldsymbol{a}_{\mathrm{d}}$ is the atmospheric drag acceleration. $\|\cdot\|$ represents the 2-norm. In the ECI frame, $J_2 = 1.0826269 \times 10^{-3}$ and the acceleration of the J_2 perturbance is

$$\boldsymbol{a}_{J_2} = \frac{3}{2}\frac{\mu J_2 R_{\mathrm{E}}^2}{r^5}\begin{bmatrix} \frac{5xz^2}{r^2} - x \\ \frac{5yz^2}{r^2} - y \\ \frac{5z^3}{r^2} - 3z \end{bmatrix} \tag{2}$$

where $R_{\mathrm{E}} = 6378.137\,\mathrm{km}$ is the radius of the Earth.

In the ECI frame, $\boldsymbol{a}_{\mathrm{d}}$ can be approximated as

$$\boldsymbol{a}_{\mathrm{d}} = -\frac{1}{2}C_{\mathrm{d}}\rho\left(\frac{S}{m}\right)v_{\mathrm{r}}\boldsymbol{v}_{\mathrm{r}} \tag{3}$$

where C_{d} is the atmospheric drag coefficient, S is the upwind area of the satellite, m is the mass of the satellite, and ρ is the atmospheric density. The 1976 standard atmosphere model is used here, so ρ is only related to the orbital altitude of the satellite. $\boldsymbol{v}_{\mathrm{r}}$ is the velocity vector of the center of mass of the satellite with respect to the local atmosphere and $v_{\mathrm{r}} = \|\boldsymbol{v}_{\mathrm{r}}\|$, i.e.,

$$\boldsymbol{v}_{\mathrm{r}} = \boldsymbol{v} - \boldsymbol{\omega}_{\mathrm{E}} \times \boldsymbol{r} = \begin{bmatrix} v_x + \omega_{\mathrm{E}} y \\ v_y - \omega_{\mathrm{E}} x \\ v_z \end{bmatrix} \tag{4}$$

where $\boldsymbol{\omega}_{\mathrm{E}} = [0, 0, \omega_{\mathrm{E}}]^{\mathrm{T}}$ is the Earth's rate of rotation, $\omega_{\mathrm{E}} = 7.2921158553 \times 10^{-5}\,\mathrm{rad/s}$.

The impulse vector in the ECI frame is $\Delta\boldsymbol{v}$, and the moments before and after the impulse are denoted by t^- and t^+, respectively. The position and velocity vectors satisfy the following equation:

$$\begin{cases} \boldsymbol{r}\left(t^+\right) = \boldsymbol{r}\left(t^-\right) \\ \boldsymbol{v}\left(t^+\right) = \boldsymbol{v}\left(t^-\right) + \Delta\boldsymbol{v}. \end{cases} \tag{5}$$

The mass change of the observation satellite before and after the impulse satisfies

$$m\left(t^+\right) = m\left(t^-\right)\exp\left(-\frac{\Delta v}{g_0 I_{\mathrm{sp}}}\right) \tag{6}$$

where $\Delta v = \|\Delta\boldsymbol{v}\|$ is the impulse magnitude, I_{sp} is the specific impulse, and $g_0 = 9.80665\,\mathrm{m/s}^2$ is the acceleration due to gravity at sea level.

A target is said to be observed if the target enters the view field of the camera. Without loss of generality, it is assumed that the view field of the camera on each satellite is determined by the line-of-sight angle γ. Each camera is assumed to point to the center of the Earth, and the line-of-sight angle is defined as the angle between $\boldsymbol{r}_{\mathrm{obs}}$ and $\boldsymbol{r}_{\mathrm{obs}} - \boldsymbol{r}_{\mathrm{tar}}$, where $\boldsymbol{r}_{\mathrm{tar}}$ and $\boldsymbol{r}_{\mathrm{obs}}$ are the position vectors of the ground target and the observation satellite in the ECI frame, respectively.

B. Constraints

1) *Mission Constraint:* All targets need to be observed, and each target should be visited only once. The mission must be completed before $t_{\max}$.

2) *Fuel Constraint:* The mass $m^{\{k\}}$ of the kth satellite is made up of dry weight, $m_0^{\{k\}}$, and the fuel load weight, $m_{\mathrm{fuel}}^{\{k\}}$. During the mission, no satellite should run out of fuel.

3) *Satellite Maneuverability Constraint:* Limited by the capacity of the thrusters, Δv is less than or equal to $\Delta v_{\max}$, and the time interval between two adjacent impulses of each satellite must be no less than $\Delta t_{\min}$.

4) *Altitude Constraint:* During the task, the orbital altitude of each satellite needs to be no less than $h_{\min}$; otherwise, the satellite is considered to have hit the Earth. To ensure the imaging quality, the orbital altitude of the observation satellites should be less than $h_{\max}$ during the observation period.

5) *Observation Constraint:* Satellites can be equipped with infrared cameras or optical cameras (we refer to these as infrared satellites or optical satellites, respectively, in the following). The observation task is performed when the target enters the view field of the camera of the kth satellite, $\gamma_{\max}^{\{k\}}$. The observation data are only valid if the solar elevation angle of the target β is no lower than $\beta_{\min}$ for optical satellites, whereas infrared satellites are not affected by the solar elevation angle.

6) *Data Transmission Constraint:* Due to the limited storage capacity of satellites, the observation data should be transmitted at a suitable time. Data transmission from an observation satellite to any relay satellite is necessary after observing N_{data} targets at most. The data transmission, which takes t_{data}, is performed when the distance between the observing satellite and the relay satellite is less than r_{data}.

The mathematical expressions of the aforementioned constraints are as follows:

$$\bigcup_{k=1}^{K}\left\{o \mid o = o_j^{\{k\}},\, j \in \left[1, J^{\{k\}}\right]\right\} = \{o_1, o_2, \ldots, o_N\} \tag{7}$$

$$\sum_{k=1}^{K}\sum_{j=1}^{J} o_j^{\{k\}} = N \tag{8}$$

$$m^{\{k\}}(t_{\max}) \geq m_o^{\{k\}} \tag{9}$$

$$\Delta v_i^{\{k\}} \leq \Delta v_{\max},\, i = 1, 2, \ldots, I^{\{k\}} \tag{10}$$

$$t_{\Delta v_{j+1}}^{\{k\}} - t_{\Delta v_j}^{\{k\}} \geq \Delta t_{\min} \tag{11}$$

$$h^{\{k\}}(t) \geq \Delta h_{\min},\, t \in [t_s, t_{\max}] \tag{12}$$

$$h_j^{\{k\}} \leq \Delta h_{\max} \tag{13}$$

$$\gamma_j^{\{k\}} \leq \gamma_{\max}^{\{k\}} \tag{14}$$

$$\beta_j^{\{k\}} \geq \beta_{\min} \tag{15}$$

$$\sum_j o_j^{\{k\}} = N_{\text{data}}, t_{o_j}^{\{k\}} \in \left[t_{d_m}^{\{k\}}, t_{d_{m+1}}^{\{k\}}\right] \tag{16}$$

$$\left\|\boldsymbol{r}_{\text{sat}}(t) - \boldsymbol{r}_{\text{relay}}(t)\right\| \le r_{\text{data}}, t \in \left[t_{d_m}^{\{k\}}, t_{d_m}^{\{k\}} + t_{\text{data}}\right]. \tag{17}$$

C. Performance Index

A general multisatellite responsiveness scheduling mission should take into account the combined effects of the revisit time, imaging quality, and fuel consumption. Thus, a general form of the performance index is defined as

$$\max J = \sum_{i=1}^{N} f(t_i, h_i, m_i). \tag{18}$$

Specific forms of the performance index need to be developed by the task requirements, which will be introduced in Sections IV and V.

III. MTS FRAMEWORK

For the problem under discussion, it is difficult to give an optimal or even feasible solution for the following reasons.

1) The target distribution, observation sequence optimization, and data transmission scheduling problems are each combinatorial optimization problems that are NP-hard. Thus, the multisatellite responsiveness scheduling problem with these three subproblems has a vast search space.
2) There are too many constraints. For example, during the observation process, the data transmission to the relay satellites should be considered.

Additionally, even the number of maneuvers (the number of optimization variables) cannot be determined in advance, resulting in a relatively small feasible region of the problem. Thus, it is difficult for optimization algorithms to obtain feasible solutions, significantly increasing the optimization difficulty.

In this section, the MTS framework is used to address this problem by simultaneously completing the target distribution and observation sequence optimization tasks. Different from a traditional tree search, MTS contains multiple trees corresponding to the number of satellites. Each node in a tree represents a state of a satellite, and each tree represents all the state information of each satellite over the mission time. In the MTS framework, the TNC is defined as a collection of corresponding nodes in each tree that represents the current state of each satellite under the current layer. When expanding the tree, the expansion object is no longer a node but a TNC composed of corresponding nodes.

After this processing, all tree search algorithms, e.g., breadth-first or depth-first search, beam search, branch and bound search, and Monte Carlo tree search, can be used in the framework. Note that the TNC is placed in the expanding list of each algorithm. In this article, we use the beam search, which performs well in complex optimization problems [27]–[30] despite being an incomplete search algorithm (i.e., the globally optimal solution is not guaranteed).

```
Initialize system parameters
Initialize root nodes in each tree
Assemble them into root TNC and put it into expand list
while ( expand list not empty)
   layer = layer + 1
   for each TNC in expand list
      determine node i to be expanded by g
      expand node i
      assemble leaf nodes of node i with nodes in other
trees into new TNCs
      add new TNCs into generation list
   end for
      sort generation list by h_e and save top W TNCs in
expand list
      clear generation list
end while
```

Fig. 2. Pseudocode of MTS framework with beam search.

The beam search procedure involves expansion and selection stages: during the expansion stage, nodes in the current layer can expand leaf nodes according to rules and constraints. Then, in the selection stage, all leaf nodes are evaluated in terms of their rewards, and the top W nodes are selected for the next layer of expansion. The other leaf nodes are pruned to reduce the search space. W is called the beam width, and is used to measure the search ability.

In summary, the MTS framework is an extension of the original tree search framework. Existing tree search algorithms can be directly applied in the MTS framework, while the object at the expansion phase is the TNC containing multiple nodes. When there is only one satellite (i.e., the number of nodes in each TNC is 1), MTS degenerates into a traditional tree search framework. There are two critical points of MTS that need to be explained in detail. The first concerns how the TNC and its corresponding nodes expand during the expansion phase; the second is how the leaf nodes generated and the detailed settings required to handle the constraints of the scheduling problem. These descriptions are given in the following subsections.

A. Expansion

For the multisatellite responsiveness scheduling problem, every node represents one observation behavior, and only one node in each TNC will be expanded, thus ensuring that nodes in the same layer have observed the same number of targets and facilitating the comparison of each node's reward. Since there are multiple nodes in a single TNC, one node needs to be determined to be later expanded. Here, in this article, we defined the rule g, which is the last observation epoch, to choose the node as shown in the left part of Fig. 3. That is, the node in TNC with the smallest last observation epoch will be selected. This design of g is to make the observation epochs represented by the nodes in the TNC as close as possible so that satellites can perform observations in a parallel and cooperative way.

When the node i is expanded, each newly expanded node, together with the nodes of the other trees in the

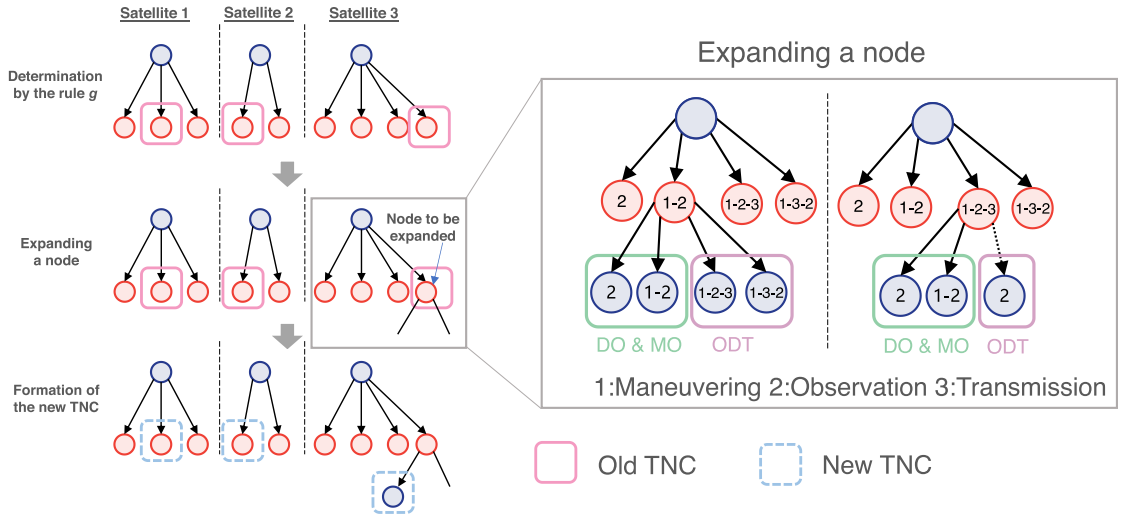

Fig. 3. Schematic diagram of expansion in MTS. "DO," "MO," and "ODT" represent three observation behaviors: direct observation, maneuvering observation, observation before or after data transmission, respectively.

original TNC, forms a new TNC that is placed in a temporary generation list. Parallel processing technology is used here to speed up the search. After the expansion phase, the TNCs in the generation list are sorted in descending order according to the heuristic function h_e, and the top W are selected and placed back into the expansion list. The pseudocode of the whole procedure of MTS with beam search is shown in Fig. 2. The form of the heuristic function h_e is significant in the beam search, although its design depends heavily on the specific problem. A good selection of h_e makes it easier to find the optimal solution. In the numerical experiment of the CTOC11 task 1, we provide an example of the design of h_e and give a brief explanation.

B. Leaf Nodes

In the MTS framework, the handling constraints are embedded in the expansion process. When the satellite should take maneuvers, the orbit elements of the satellite are propagated according to (24) until constraint (11) is satisfied at the beginning of the expanding node. Through the aforementioned processing, the maneuvering time interval constraint is naturally satisfied. The newly expanded nodes are traversed to determine whether they satisfy constraints (11)–(16). If a conflict arises, the corresponding node will not be used to form a new TNC. After such constraints have been considered, the remaining TNCs in the generation list are feasible.

Expanding a node means that the satellite completes an observation behavior of one unobserved target. This article considers the following three possible observation behaviors:

1) Direct observation.
2) Maneuvering observation.
3) Observation before or after data transmission.

The right part of Fig. 3 shows the three observation behaviors of expanding nodes. In Fig. 3, we use numbers to simplify the expression of actions: "1" for implementing a maneuver, "2" for observing a target, and "3" for starting to transmit data. The order of the numbers is the order in which the actions are performed.

Direct observation, as the name implies, observes a target without any maneuvering. Although the opportunity for this scenario is much smaller than for the second scenario, the probability should not be negligible, especially when $\Delta t_{\min}$ is large.

Maneuvering observation means that the satellite must rely on its own maneuverability to observe a prescribed target. This can dramatically shorten the time required for observation, but the maneuver method (transfer time and direction of maneuver) makes the scheduling problem more sophisticated. To reduce the enormous search space, we adopt an analytical solution for a single coplanar impulsive maneuver (considering linear J_2 perturbation) [22] to obtain an initial guess, which is then refined in the dynamics equation (1). The details of analytical solution can be found in[22]. Note that there are multiple possible maneuvers that would enable a given target to be observed. In this case, a local optimal solution may not be the global optimal solution, taking into account other constraints. In the proposed method, different nodes are expanded to consider the various situations of the maneuver method (such as the descending or ascending ground track).

The third observation behavior involves determining how to finish data transmission through orbit maneuvering. The observation situation will then be considered, given that each node represents one observation behavior. The observation situation can be divided into two cases: observation before or after data transmission. For the first case, some specific targets will be completed incidentally, further reducing the task completion time. For the second case, the first two observation behaviors can continue to be used. In the right part of Fig. 3, the dashed arrow represents a special situation in observation before or after

TABLE I
Initial Orbital Elements of Satellites

ID	a (km)	e	i (°)	Ω (°)	ω (°)	f (°)
FENGYUN 3A	7211	0.0023	98.4	355.3	97.8	287.8
FENGYUN 3B	7216	0.0028	99.0	340.0	39.6	180.4
FENGYUN 3C	7215	0.0009	98.7	57.6	69.3	245.9
FENGYUN 3D	7210	0.0008	98.6	302.1	77.8	268.8
FENGYUN 3E	7172	0.0023	98.7	3.8	57.7	229.3

TABLE II
Twenty Randomly Selected Targets

Target	longitude	laitude	Target	longitude	laitude
Buenos Aires	−60.0°	−36.3°	Washington	−77.0°	39.9°
Cairo	31.1°	30.0°	Mexico City	−99.1°	19.2°
Canberra	149.1°	−35.2°	Ankara	32.5°	39.6°
Brasilia	−47.6°	−15.5°	Tehran	51.3°	35.4°
Warszawa	21.0°	52.1°	Roma	12.3°	41.5°
Berlin	13.3°	52.3°	New Delhi	77.1°	28.4°
Moscow	37.4°	55.5°	London	−0.1°	51.4°
Paris	2.2°	48.5°	Beijing	116.2°	39.6°
Maynila	121.0°	14.4°	Tokyo	139.8°	35.6°
Ottawa	−75.4°	45.3°	Johannesburg	28.2°	−25.8°

data transmission. Since this expanded node ("1-2-3") has completed the data transmission, the satellite will no longer take additional maneuvers but a direct observation. That is, the actions represented by this expanded node ("1-2-3") and the leaf node ("2"), arranged in chronological order, should be "1-2-2-3." Section V provides detailed information about the maneuver methods used to complete data transmission with the relay satellite.

IV. CASE 1: SIMPLIFIED SCENARIO COMPARED WITH OTHER ALGORITHMS

In this section, a simplified scenario (ignoring some constraints) for the scheduling of a multisatellite response was simulated to fully demonstrate the search process used by MTS. Compared with GA and ACO optimization algorithms, the simulation results show that MTS was more effective.

A. Scenario Description

In this test scenario, five satellites equipped with infrared sensors observed 20 ground targets. Details of the satellites and target points are listed in Tables I and II, respectively. The task starts at 2020-1-1 00:00:00 (UTC). The corresponding Julian day and Greenwich mean sidereal time are

$$JD_0 = 2458849.5,\ \alpha_{G0} = 1.747455428309031\,\text{rad}. \quad (19)$$

To compare each optimization method more intuitively, the scenario was simplified. That is, the orbital altitude of the satellite could not be lower than 200 km during the whole mission. No other constraints were considered. Initially, the total mass of a satellite was set to 1000 kg, and the view field of the infrared sensor was 2.5°.

The performance index for this scenario has two forms. The first is the shortest observation time

$$\max J = \frac{1}{t_{\text{end}}} \quad (20)$$

where t_{end} is the last target observation time.

The second is a comprehensive consideration of the task completion time, fuel consumption, and observation quality

$$\max J = \frac{\sum_{i=1}^{5} m_{\text{end}}^{\{i\}}}{t_{\text{end}} h_{\text{avg}}} \quad (21)$$

where $m_{\text{end}}^{\{i\}}$ is the remaining mass of the ith satellite after the mission ends, and h_{avg} is the average value of each observation altitude.

B. Search Process in MTS

To make it easier to apply the other optimization algorithms in this scenario, only the pulse with the minimum velocity increment in one day of observation was considered. The next pulse was immediately carried out after the observation, as in [20], [23]. After the aforementioned processing, there were $20! \times 5^{20}$ possible solutions in the state space of this scenario. That is, the optimization variables are the observation sequence of all targets and the ID of the observation satellite for each target. This problem can be regarded as a multitraveling salesman problem (MTSP).

As this is a simplified scenario, expanding a leaf node in MTS needs to consider only the "maneuvering observation" case. Rule g in MTS uniformly adopts the smallest last observation epoch of the node in TNC, as mentioned in Section III.

The heuristic function h_e corresponding to the first form of the performance index (20) is defined as

$$h_e = \frac{1}{t_{\text{last}}} \quad (22)$$

where t_{last} is the time epoch of the last observation of each node in the current layer. Here, $t_{\text{end}} = t_{\text{last}}$ when observing the last target.

The heuristic function h_e corresponding to the second form (21) is defined as

$$h_e = \frac{\sum_{i=1}^{5} m_{\text{last}}^{\{i\}}}{t_{\text{last}} h_{\text{avg}}} \quad (23)$$

where $m_{\text{last}}^{\{i\}}$ is the remaining mass of the ith satellite in the current layer.

C. Comparison With Other Algorithms

In this section, we compare the efficacy of MTS to that of the optimization algorithms GA [31] and ACO [32], [33]. For GA and ACO, each test in the simplified scenario was run repeatedly 20 times. MTS was run only once because the result is deterministic. The tests were run on an Intel Xeon Gold 6148 processor with 40 cores at 2.4 GHz. To ensure the comparison was fair, each method was given about 30 minutes to run.

TABLE III
Results of GA, ACO, and MTS

	Algorithm	Options	J_{avg}	var	t_{avg}(min)	J_{best}	m_{best}(kg)	h_{best}(km)	t_{best} (day)
$J=\frac{1}{t_{\text{end}}}$	GA	$n=250, iter=100$	0.51	0.0013	27.0	0.59	4563.7	829.8	1.7
	ACO	$n=100, iter=40$	0.65	0.0033	24.0	0.74	4715.0	880.8	1.4
	MTS	$W=18,000$	0.83	/	30.6	0.83	4644.9	899.1	1.2
$J=\frac{\sum_{i=1}^{5} m_{\text{end}}^{\{i\}}}{t_{\text{end}} h_{\text{avg}}}$	GA	$n=250, iter=100$	3.95	0.1377	31.8	4.99	4593.6	442.1	2.1
	ACO	$n=100, iter=40$	4.61	0.1883	25.5	5.47	4614.8	607.4	1.4
	MTS	$W=18,000$	6.46	/	31.2	6.46	4658.3	450.7	1.6

1) *Genetic Algorithm (GA):* Two-chromosome and related operators for the MTSP [31] were used. The crossover and mutation rates were 0.75 and 0.05, respectively. The crossovers and mutations were performed the same as in [31]. The population size and the number of iterations were 250 and 100, respectively.

2) *Ant Colony Optimization (ACO):* The basic method and values in the pheromone matrix were the same as in [32]. As an adaptation of the MTSP, before departure, each ant was randomly allocated a number of cities to observe with each satellite. The list of cities was reset for each iteration [33]. The heuristic value (in [32]) uses $1/\Delta t_{i,j}$ and $h_j/(\Delta m_{i,j}\Delta t_{i,j})$ for the two forms of the performance index. Here, $\Delta t_{i,j}$ and $\Delta m_{i,j}$, respectively, represent the time and fuel costs for a satellite to switch from target i to target j. h_j is the altitude when observing target j. The other parameters were set the same as in [33]. The number of ants and number of iterations were 100 and 40, respectively.

The results of GA, ACO, and MTS are compared in Table III. n is the population size or number of ants and $iter$ is the number of iterations. J_{avg} and J_{bset} are the average value and best value of the performance index, respectively. var is the variance of the 20 results, and t_{avg} is the average real computation time. m_{best}, h_{best}, and t_{best} are the remaining mass for the five satellites, the average observation altitude, and the mission completion time for the best result found by each algorithm. The best results for the two forms of the performance index were both obtained by MTS. J_{best} was 0.83–6.46 for MTS, 0.59–4.99 for GA, and 0.74–5.47 for ACO.

V. CASE 2: CTOC11 TASK 1

In this section, one sophisticated scenario of the multisatellite responsiveness scheduling mission (CTOC11 task 1) was simulated to assess the effectiveness of the proposed algorithm. The description of the scenario and the experimental results are presented as follows.

A. Scenario Description

The test scenario: Two observation satellites complete the observation of 200 ground stationary targets. Teams participating in the competition needed to design the orbit and optimize the maneuvers of these two satellites. One satellite is equipped with an infrared camera and the other has an optical camera. Each satellite obtains a different single-target score after completing one observation. During the mission, the transmission of observation data to one of the relay satellites is considered. The task starts at 2020-1-1 00:00:00 (UTC).

At the beginning of the task, the two observation satellites are in a circular orbit with an orbital altitude of 350 km and the same initial orbital plane. The other orbit elements must be designed. In this article, we directly set the orbital inclination of the two satellites corresponding to the maximum latitude of the ground targets. Thus, the initial orbit elements to be designed are the ascending node right ascension of the two satellites and the true anomaly of each satellite. As for the orbit design, the algorithm starts as a virtual root node, and feasible first-layer nodes are expanded discretely according to the orbital elements. More details can be found in the appendix. Other relevant parameters are given in Table IV.

The performance index in the CTOC11 task 1 is defined as

$$\max J = A\frac{t_{\max}}{t_{\text{end}}}\sum_{i=1}^{N}\frac{s_i}{t_{\text{end}}/86400+(t_i/86400)^2} \tag{24}$$

where J is the score for task 1, $A=14$ is the proportionality factor of task 1 to other tasks, t_i the observation time of target point i and $t_{\max}=60\times 86400$ s. The faster task 1 can be completed, the higher the score. s_i is the observation score of the target point i, which is defined as

$$s = C(5-0.01\,h) \tag{25}$$

where $h=r-R_E$ is the orbital altitude of the observation satellite during its observation and $h\in[200,500]$ km. C is the camera coefficient, which is determined by the type of camera. In CTOC11, $C=1$ for the optical camera and $C=0.8$ for the infrared camera.

B. Maneuvering for Data Transmission With Relay Satellites

As mentioned previously, the method used for maneuvering observation is taken from [22]. The following describes the method of maneuvering for data transmission. There are four relay satellites for communication. Only the gravity and J2 perturbation are considered in the dynamics of the relay satellites, as their high orbital altitude weakens the effect of atmospheric drag. The initial instantaneous orbital elements of the four relay satellites are shown in Table V, where a is the semimajor axis, e is the eccentricity,

TABLE IV
Parameter Settings of CTOC11 Task 1

Parameter	S	C_{d}	m_0	m_{fuel}	I_{sp}	$\gamma_{\max}$	$\Delta t_{\min}$	$\Delta v_{\max}$	$h_{\min}$	$h_{\max}$	β	N_{data}	t_{data}	r_{data}
Value	8	2	300	250	300	2.5	0.5	0.1	200	500	20	30	10	100
Units	m^2	/	kg	kg	s	$^\circ$	day	km/s	km	km	$^\circ$	/	s	km

TABLE V
Initial Orbital Elements of Relay Satellites

ID	a (km)	e	i ($^\circ$)	Ω ($^\circ$)	ω ($^\circ$)	f ($^\circ$)
1	16763	0.5957	63.4	0	270	0
2	16763	0.5957	63.4	90	270	0
3	16763	0.5957	63.4	180	270	0
4	16763	0.5957	63.4	270	270	0

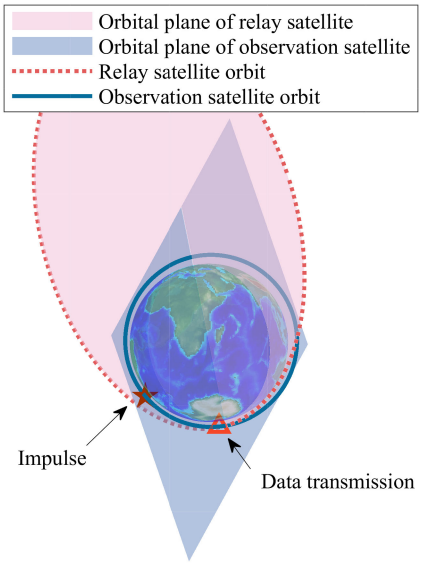

Fig. 4. Illustration of maneuvering for data transmission.

i is the orbital inclination, Ω is the right ascension of the ascending node, ω is the perigee angle, and f is the true anomaly.

The method of in-plane impulse is adopted. First, under the two-body dynamics model, the two intersection points between the satellite orbital plane and each relay satellite orbit are calculated. Second, the Lambert problem is used to find Δv of the intersection at a lower altitude. Fig. 4 shows the geometric relationship between the observing satellite and the relay satellite. The triangle in Fig. 4 denotes the position of the intersection, and the pentagram is the position of the satellite when it pulses. The maneuvering epoch in this process, a continuous optimization variable, is obtained by uniformly discretizing the next two days and computing twice the number of revolutions of the satellite over this period. Third, take all these solutions as initial guesses and substitute them into the nonlinear programming algorithm, and find the globally time-optimal solution through comparison. Finally, such a solution is refined into the dynamics equation (1) iteratively.

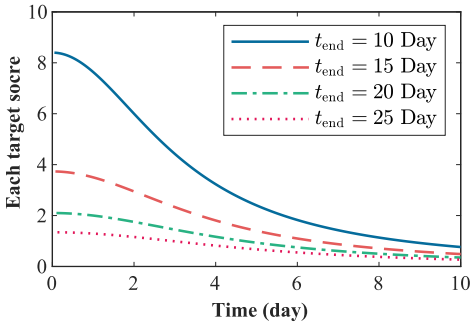

Fig. 5. Approximate performance index of different t_{end} .

TABLE VI
Results of CTOC11 Task 1

Algorithm	Options	Score	$m_{f,o} - m_{f,i}$	t_{end}
MTS	$t_x = 0$	325	422-384	16.1
MTS	$t_x = 1$ day	382	379-396	17.2
MTS	$t_x = 2$ days	**387**	**402-422**	17.5
MTS	$t_x = 3$ days	350	421-390	18.8

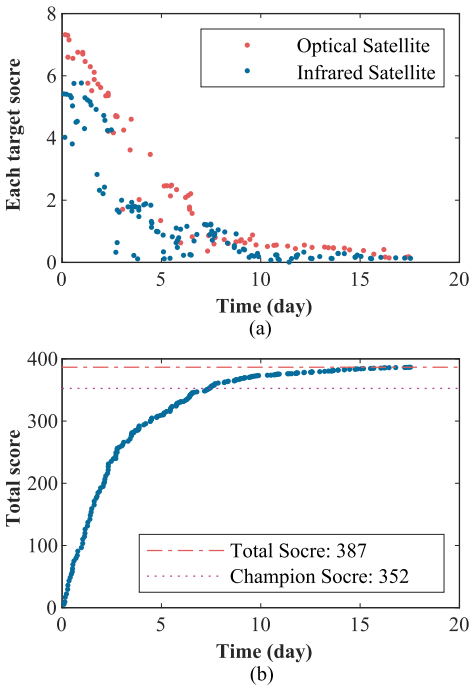

Fig. 6. Best solution ($J_{\mathrm{best}} = 387$). (a) Each target score over time. (b) Total score over time.

C. Design of the Heuristic Function h_e

As a general rule, the heuristic function h_e in the beam search algorithm can be defined as the partial total performance index, but it is sometimes impossible to find

TABLE VII
Best Solution Found by MTS

Initial orbit element$(a, e, i, \Omega, \omega + f)$	Optical satellite: 6728.137 km, 0, 115.8°, 62.0°, 342.0° Infrared satellite: 6728.137 km, 0, 115.8°, 62.0°, 338.4°
Optical satellite sequence	117 2 45 37 161 132 104 54 168 56 179 148 158 35 157 96 48 6 14 195 64 127 120 52 135 101 89 189 124 185 (1004) 44 196 119 190 128 95 79 65 198 151 199 85 187 60 41 23 138 19 87 162 165 78 33 62 5 24 3 15 68 34 (1004) 171 18 184 159 169 43 136 80 133 100 145 118 183 38 72 197 180 139 20 (1001)
Infrared satellite sequence	176 156 113 122 10 166 126 27 181 29 130 66 177 59 16 108 74 8 97 150 22 30 28 107 26 98 160 170 17 140 (1004) 93 94 84 31 191 146 121 4 69 92 25 142 53 109 73 155 71 47 192 90 137 164 173 154 188 114 194 (1004) 55 42 7 175 50 12 129 141 125 106 70 75 163 40 152 167 36 182 131 57 67 102 76 82 105 58 49 99 (1004) 39 123 46 200 86 21 13 11 111 186 91 147 153 83 149 9 81 112 134 88 174 61 172 115 77 (1004) 110 116 63 143 144 1 32 103 193 51 178 (1004)

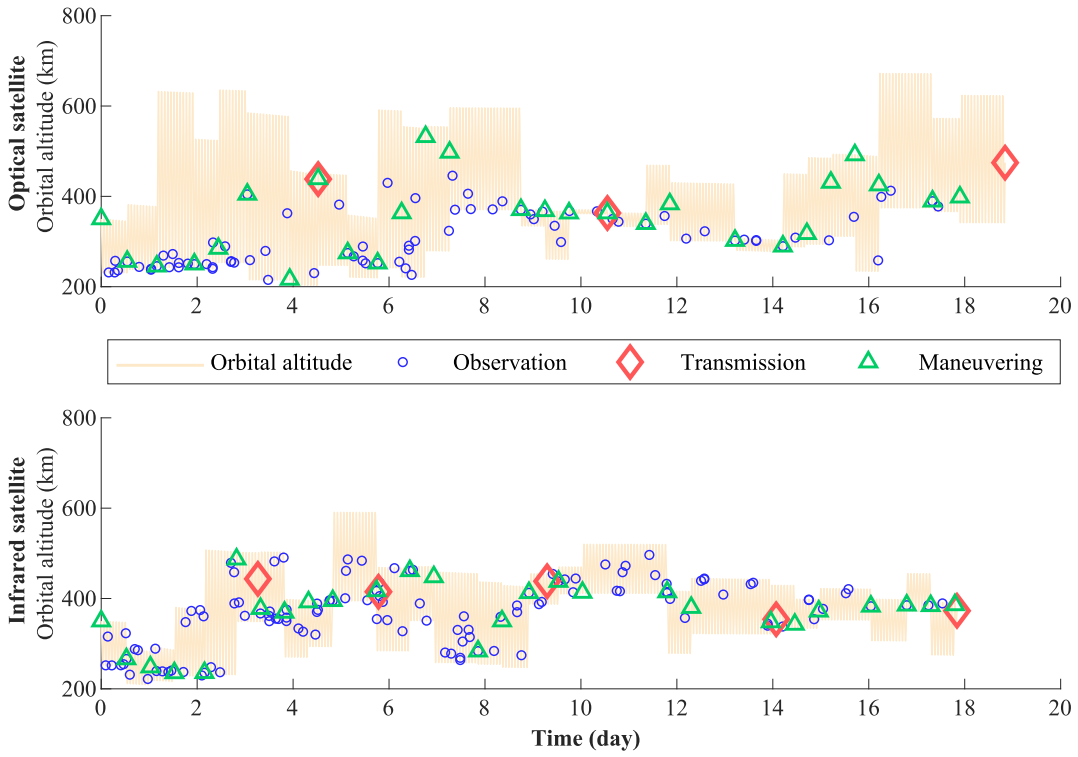

Fig. 7. Action sequence of the best solution found by MTS.

h_e directly. Here, we present an example of the design of h_e in such a case by two steps.

1) *The first step:* In task 1, t_{end} in the performance index, given by (24), cannot be determined until the solution has been found. Therefore, the heuristic function h_e should be modified during the beam search process. In this article, we present an approximate estimate of t_{end} after analyzing the performance index (24). Fig. 5 shows the effect of t_{end} on the performance index after setting $s_i = 1$ in (24). It is obvious that each point score falls dramatically over time, where the rate of decline reaches its peak after 2–3 days, and such a trend becomes increasingly evident as t_{end} decreases. It is reasonable to conclude that the major contribution to the score is obtained in the early observation process, while the goal of the latter observations is to shorten t_{end}. Accordingly, the two-stage estimate of t_{end} is defined as

$$t_{\text{end}} = \begin{cases} t_x, & t_{\text{last}} < t_x \\ t_{\text{last}}, & t_{\text{last}} \geq t_x \end{cases} \tag{26}$$

where t_x is a design parameter that balances the conflict between early scoring and task completion. When t_{end} is in the first situation of (26), s_i has a greater impact on the performance index (24). As a result, nodes with higher s_i are easier to be branched. When t_{last} is in the other situation, t_i has a more significant influence, so the algorithm will discard those nodes that observe more slowly so that the speed of task completion is faster.

2) *The second step:* To reduce fuel consumption, the heuristic function is chosen to satisfy the task 1 performance index and minimize the use of propellant [34]

$$h_e = J_{\text{current}}(m_{\text{optical}} + m_{\text{infrared}})^{1.5} \tag{27}$$

where J_{current} is the sum of the scores of the current observed target, t_{end} is given by (26), and m_{optical} and m_{infrared} are the current masses of the optical and infrared satellites, respectively.

The MTS results with different t_x are presented in Table VI. All four tests were run on an AMD EPYC 7H12 processor with 64 cores at 2.6 GHz. The program runs on the C++ platform. Minpack-1 [35], a nonlinear equation Solver, is used in iteration, and Nlopt [36] is used in local optimization. Due to the complexity of CTOC11 and the need to obtain the optimal solution, W was set to 70 000, and the computing time for each test was 2.9 days. As can be seen from (26), $t_x = 0$ can be regarded as a direct estimate without considering the analysis of the performance index. The results in Table VI demonstrate the importance of a reasonable design of h_e, and the prediction of t_{end} is in line with our previous analysis in Fig. 5.

D. Results and Discussion

The total score and each observation score of the best solution, which is set to $t_x = 2$ days, are given in Fig. 6. The later each target was observed, the lower the score of that observation, which explains the slow increase in the total score later in the task. In fact, the first five days of task execution contribute approximately 80% of the total score. This trend, which takes into account satellite types and observation altitude, is consistent with the previous analysis in Fig. 5.

Details of the best solution, including the initial orbital elements of the two satellites and the observation sequence, are presented in Table VII and Fig. 7. In Table VII, each number in the observation sequence corresponds to the target ID (1–200), and the number in brackets represents communication with the four corresponding relay satellites (1001–1004). From the perspective of dynamics, the observation satellites find it easier to communicate with the relay satellites at some specific locations, as evidenced by the solutions: the infrared satellite only communicates after the first observation of 30 targets, with less than 30 targets remaining. In Fig. 7, the straight line represents the state of the satellite in the environment, the circles denote the observations, the triangles are orbit maneuvers, and the diamonds denote the start of data transmission. Obviously, the two satellites drop to a lower orbit at the beginning of the task to gain higher scores, which reveals the effectiveness of the proposed framework. Compared with the solution of the winning CTOC11 team, the best solution given by the proposed method obtains a higher score (387) and has a faster completion time (17.5 days), but also preserves the similar amount of fuel (276 kg consumed altogether) across the two satellites after completing task 1. For the winning solution, the task was completed within 19.2 days with a score of 352, and 269 kg of fuel was consumed. Based on the new solution to task 1 found by MTS, the total performance index for completing the whole CTOC11 was 635 (which exceeded the score of the winning team by 33 points).

In this competition, the champion team first used the mass of the satellite, semimajor axis, inclination, eccentricity, and perigee parameters to fit the ground track, and then, established a table of discrete time steps according to the minimum satellite maneuver interval $\Delta t_{\min}$. Finally, the mission scheduling was carried out according to the table. With their method, it is more difficult to deal with the situation where $\Delta t_{\min}$ is changing. Our proposed framework not only achieves better results but is also more general than the winning team's method.

VI. CONCLUSION

Related research focuses on the rapid response of a single satellite. This is the first article to systematically analyze and describe the scheduling problem for a multisatellite response. Moreover, it gives a solution for the whole process. This article provides a more practical and powerful proof for the operational responsiveness in space of a multisatellite network.

In this article, a heuristic and effective framework MTS is proposed for solving the multisatellite responsiveness scheduling problem. A novel idea for constructing multiple trees and TNCs is used to extend the traditional tree search framework so that the target distribution, observation sequence, and data transmission of each satellite are optimized simultaneously. We then use the beam search and parallel processing technology to solve this global optimization problem and facilitate large-scale computing during the expansion. In addition, the existing ground-track adjustment technique is adopted to overfly the next target at the node expansion phase.

This article compares MTS with other algorithms (GA and ACO) and demonstrates that the proposed method is effective. Moreover, MTS found a new best solution to task 1 of CTOC11 (200 targets to be observed within 18 days by two Earth observation satellites).

In this article, only J2 perturbation and atmospheric drag have been considered in the dynamic model, but it can be relatively simple to extend this to a higher precision model. Furthermore, the proposed framework can be used in other multispacecraft multitarget sequence optimization problems, such as the active space debris removal problem, which will be studied in future research.

APPENDIX
INITIAL ORBIT DESIGN

In the requirements of the CTOC11, the initial orbital elements of the two satellites need to be designed (orbital inclination, right ascension of the ascending node, and phase angle). Since choosing these orbital elements significantly affects the completion of subsequent tasks, a theoretical

analysis is needed to substantially reduce the search space and improve the performance index. Therefore, the following preanalysis is necessary.

A. Inclination

For all targets to be observed, the maximum latitude is 64.2°. The orbital inclination must be in [64.2°, 115.8°] for the satellite to be able to observe all target points. The two orbits at the boundary are best because moving a satellite to a higher latitude would reduce its observational capability. The only difference between the two orbits is that one is prograde, whereas the other is retrograde.

The prograde orbit is affected by the J2 perturbation, and the drift direction of the right ascension of the ascending node is opposite to that of the Earth's twilight line. The prograde orbit of the optical satellite, limited by the solar elevation angle, changes from meeting the observation constraint within a half orbit to being almost unable to make observations (the orbital plane is close to the Earth's twilight line) in about 18 days.

The situation is the opposite for the retrograde orbit. With a reasonable set of right ascension values of the ascending node, the optical satellite can maintain a relatively high observation time for the first 20 days, which is enough to complete task 1. So, we chose a retrograde orbit; that is, the inclination angle is 115.8°.

B. Other Orbital Elements

For task 1, to ensure that there is enough observation time for the optical satellite in the first 20 days, we calculated that the ascending node of the satellite's orbit can meet the requirements if it is within [40°, 120°].

The next step is to find the right ascension of the ascending node and the phase angle. Since a tree search cannot optimize continuous variables, we discretized these orbit elements, using discrete steps of 0.2° for the right ascension of the ascending node and 3.6° for the phase angle of the two satellites.

In the algorithms, the root node is set since the virtual node does not contain any information. The root node then generates various orbits as child nodes based on discrete orbital elements and forms the initial TNCs ($400 \times 100 \times 100$). Then, using MTS, the final result and the specific initial orbit are obtained.

REFERENCES

[1] S. Voigt *et al.*
Global trends in satellite-based emergency mapping
Science, vol. 353, no. 6296, pp. 247–252, 2016.

[2] G. Denis
Towards disruptions in Earth observation? New Earth observation systems and markets evolution: Possible scenarios and impacts
Acta Astronautica, vol. 137, pp. 415–433, 2017. [Online]. Available: http://dx.doi.org/10.1016/j.actaastro.2017.04.034

[3] M. Yin, J. Li, X. Wang, and H. Baoyin
A rapid method for validation and visualization of agile Earth-observation satellites scheduling
Astrodynamics, vol. 2, no. 4, pp. 325–337, 2018.

[4] Z. Zhang, N. Zhang, and Z. Feng
Multi-satellite control resource scheduling based on ant colony optimization
Expert Syst. With Appl., vol. 41, no. 6, pp. 2816–2823, 2014. [Online]. Available: http://dx.doi.org/10.1016/j.eswa.2013.10.014

[5] M. Lemaître, G. Verfaillie, F. Jouhaud, J. M. Lachiver, and N. Bataille
Selecting and scheduling observations of agile satellites
Aerosp. Sci. Technol., vol. 6, no. 5, pp. 367–381, 2002.

[6] J. Wang, X. Zhu, D. Qiu, and L. T. Yang
Dynamic scheduling for emergency tasks on distributed imaging satellites with task merging
IEEE Trans. Parallel Distrib. Syst., vol. 25, no. 9, pp. 2275–2285, Sep. 2014.

[7] Y. Xu, X. Liu, R. He, and Y. Chen
Multi-satellite scheduling framework and algorithm for very large area observation
Acta Astronautica, vol. 167, pp. 93–107, Feb. 2020.

[8] E. Zhibo, R. Shi, L. Gan, H. Baoyin, and J. Li
Multi-satellites imaging scheduling using individual reconfiguration based integer coding genetic algorithm
Acta Astronautica, vol. 178, no. Jun. 2020, pp. 645–657, 2021. [Online]. Available: https://doi.org/10.1016/j.actaastro.2020.08.041

[9] Z. Li and X. Li
A multi-objective binary-encoding differential evolution algorithm for proactive scheduling of agile Earth observation satellites
Adv. Space Res., vol. 63, no. 10, pp. 3258–3269, 2019. [Online]. Available: https://doi.org/10.1016/j.asr.2019.01.043

[10] G. Wu, J. Liu, M. Ma, and D. Qiu
A two-phase scheduling method with the consideration of task clustering for Earth observing satellites
Comput. Oper. Res., vol. 40, no. 7, pp. 1884–1894, 2013. [Online]. Available: http://dx.doi.org/10.1016/j.cor.2013.02.009

[11] R. Xu, H. Chen, X. Liang, and H. Wang
Priority-based constructive algorithms for scheduling agile Earth observation satellites with total priority maximization
Expert Syst. with Appl., vol. 51, pp. 195–206, 2016.

[12] N. Bianchessi, J. F. Cordeau, J. Desrosiers, G. Laporte, and V. Raymond
A heuristic for the multi-satellite, multi-orbit and multi-user management of Earth observation satellites
Eur. J. Oper. Res., vol. 177, no. 2, pp. 750–762, 2007.

[13] M. Guelman and A. Kogan
Electric propulsion for remote sensing from low orbits
J. Guid., Control, Dyn., vol. 22, no. 2, pp. 313–321, 1999.

[14] M. Pontani and P. Teofilatto
Satellite constellations for continuous and early warning observation: A correlation-based approach
J. Guid., Control, Dyn., vol. 30, no. 4, pp. 910–920, 2007.

[15] O. Abdelkhalik and D. Mortari
Orbit design for ground surveillance using genetic algorithms
J. Guid., Control, Dyn., vol. 29, no. 5, pp. 1231–1235, 2006.

[16] M. P. Wilkins and D. Mortari
Flower constellation set theory part II: Secondary paths and equivalency
IEEE Trans. Aerosp. Electron. Syst., vol. 44, no. 3, pp. 964–976, Jul. 2008.

[17] D. Casanova, M. E. Avendano, and D. Mortari
Design of flower constellations using necklaces
IEEE Trans. Aerosp. Electron. Syst., vol. 50, no. 2, pp. 1347–1358, Apr. 2014.

[18] K. J. Zhu, J. F. Li, and H. X. Baoyin
Satellite scheduling considering maximum observation coverage time and minimum orbital transfer fuel cost
Acta Astronautica, vol. 66, no. 1-2, pp. 220–229, 2010. [Online]. Available: http://dx.doi.org/10.1016/j.actaastro.2009.05.029

[19] T. C. Co, C. Zagaris, and J. T. Black
Responsive satellites through ground track manipulation using existing technology
J. Spacecraft Rockets, vol. 50, no. 1, pp. 206–216, 2013.
[20] T. C. Co and J. T. Black
Responsiveness in low orbits using electric propulsion
J. Spacecraft Rockets, vol. 51, no. 3, pp. 938–945, 2014.
[21] J. Zhang, H. Y. Li, Y. Z. Luo, and G. J. Tang
Effects of in-track maneuver on the ground track of near-circular orbits
J. Guid., Control, Dyn., vol. 37, no. 4, pp. 1373–1378, 2014.
[22] G. Zhang, X. Cao, and D. Mortari
Analytical approximate solutions to ground track adjustment for responsive space
IEEE Trans. Aerosp. Electron. Syst., vol. 52, no. 3, pp. 1366–1383, Jun. 2016.
[23] M. M. Guelman and A. Shiryaev
Closed-loop control of Earth observation satellites
J. Spacecraft Rockets, vol. 56, no. 1, pp. 82–90, 2019.
[24] S. H. Mok and H. Bang
Optimal multi-target overflight using ground-track adjustment
J. Astronautical Sci., vol. 68, pp. 150–171, 2021.
[25] H. Zhang and G. Zhang
Reachable domain of ground track with a single impulse
IEEE Trans. Aerosp. Electron. Syst., vol. 57, no. 2, pp. 1105–1122, Apr. 2021.
[26] X. Lin, G. Zhang, and H. Zhang
Multi-target ground-track adjustment with a single coplanar impulse
Aerosp. Sci. Technol., vol. 119, 2021, Art. no. 107135.
[27] I. S. Grigoriev and M. P. Zapletin
Choosing promising sequences of asteroids
Automat. Remote Control, vol. 74, no. 8, pp. 1284–1296, 2013.
[28] D. Izzo, D. Hennes, L. F. Simões, and M. Märtens
Designing Complex Interplanetary Trajectories for the Global Trajectory Optimization Competitions, vol. 114. Berlin, Germany: Springer, 2016, pp. 151–176.
[29] D. Izzo, L. F. Simões, M. Märtens, G. C. De Croon, A. Heritier, and C. H. Yam
Search for a grand tour of the Jupiter Galilean moons
in *Proc. Genet. Evol. Comput. Conf.*, 2013, pp. 1301–1308.
[30] L. F. Simoes, D. Izzo, E. Haasdijk, and A. E. Eiben
Multi-rendezvous Spacecraft Trajectory Optimization With Beam P-ACO. Berlin, Germany: Springer, 2017.
[31] A. E. Carter and C. T. Ragsdale
A new approach to solving the multiple traveling salesperson problem using genetic algorithms
Eur. J. Oper. Res., vol. 175, no. 1, pp. 246–257, 2006.
[32] T. Stützle and H. H. Hoos
MAX-MIN ant system
Future Gener. Comput. Syst., vol. 16, no. 8, pp. 889–914, 2000.
[33] S. Ghafurian and N. Javadian
An ant colony algorithm for solving fixed destination multi-depot multiple traveling salesmen problems
Appl. Soft Comput. J., vol. 11, no. 1, pp. 1256–1262, 2011.
[34] H. Li, S. Chen, and H. Baoyin
J2-perturbed multitarget rendezvous optimization with low thrust
J. Guid., Control, Dyn., vol. 41, no. 3, pp. 796–802, 2018.
[35] K. E. More, and J. J. Garbow, and B. S. Hillstrom
User guide for MinPack-1
Argonne National Lab., Rep. ANL-80-74, 1980. [Online]. Available: http://www.netlib.org/minpack
[36] S. G. Johnson
The NLopt nonlinear-optimization package
2010. [Online]. Available: http://github.com/stevengj/nlopt

Zhong Zhang received the bachelor's degree in aerospace engineering, in 2019, from Tsinghua University, Beijing, China, where he is currently working toward the Ph.D. degree with the School of Aerospace Engineering.

His research interests include combinatorial optimization problems and trajectory optimization.

Nan Zhang received the bachelor's degree in engineering mechanics, in 2019, from Tsinghua University, Beijing, China, where he is currently working toward the Ph.D. degree with School of Aerospace Engineering.

He was a Visiting Student with Lunar and Planetary Laboratory, University of Arizona, from October 2018 to February 2019. His research interests include intelligent optimization algorithms for multitarget detection and trajectory optimization.

Yifei Jiao received the bachelor's degree in aerospace engineering, in 2020, from Tsinghua University, Beijing, China, where he is currently working toward the Ph.D. degree with the School of Aerospace Engineering.

His research interests include near-Earth asteroid defense and hypervelocity impact simulation.

Hexi Baoyin received the Ph.D. degree in space system engineering from the Harbin Institute of Technology, Harbin, China, in 1999.

He was a Visiting Research Fellow with the Laboratory of Advanced Space System from October 2004 to July 2005. He is currently working as a Professor with Tsinghua University. His current research interests include the orbit theory in irregular gravitational fields and interplanetary mission analysis and optimization.

Junfeng Li received the Ph.D. degree in mechanics from Moscow State University, Moscow, Russia, in 1993.

He has been a Professor with Tsinghua University, Beijing, China, since 1999. His research interests include the formation flying of spacecraft, stability theory, and orbital dynamics near small asteroids.